Use of remote sensing data to enhance the performance of a hydrodynamic simulation of a partially frozen power plant cooling lake

May V. Arsenovic[a], Carl Salvaggio[a], Alfred J. Garrett[b], Brent D. Bartlett[a], Jason W. Faulring[c], Robert L. Kremens[c], and Philip S. Salvaggio[a]

[a] Rochester Institute of Technology, Center for Imaging Science, Digital Imaging and Remote Sensing Laboratory, Rochester, New York, USA

[b] Savannah River National Laboratory, Aiken, South Carolina, USA

[c] Rochester Institute of Technology, Center for Imaging Science, Laboratory for Imaging Algorithms and Systems, Rochester, New York, USA

ABSTRACT

The effectiveness of a power generation site's cooling pond has a significant impact on the overall efficiency of a power plant. The ability to monitor a cooling pond using thermal remote sensing, coupled with hydrodynamic models, is a valuable tool for determining the driving characteristics of a cooling system. However, the thermodynamic analysis of a cooling lake can become significantly more complex when a power generation site is located in a northern climate. The heated effluent from a power plant entering a cooling lake is often not enough to keep a lake from freezing during winter months. Once the lake is partially or fully frozen, the predictive capabilities of the hydrodynamic model are weakened due to an insulating surface layer of ice and snow. Thermal imagery of a cooling pond was collected over a period of approximately 16 weeks in tandem with high-density thermal measurements both in open water and embedded in ice, meteorological data, and snow layer characterization data. The proposed research presents a method to employ thermal imagery to improve the performance of a 3-D hydrodynamic model of a power plant cooling pond in the presence of ice and snow.

Keywords: thermal infrared, hydrodynamic modeling, simulation, ice, snow, ground truth, wide-angle oblique imagery, remote sensing, ice thickness

1. INTRODUCTION

The ALGE code is a hydrodynamic model developed by Savannah River National Laboratory (SRNL) to derive the power output levels of a power generation site from observing the site's associated cooling pond with an aerial imaging platform. This research is funded by the Department of Energy with the objective of improving our ability to understand and simulate the thermodynamics and dynamics of power plant cooling lakes when they are partially frozen. When a site is located in a northern climate, the heat effluent into the cooling lake is often not enough to keep the lake from freezing during winter months. Once the lake is partially or fully frozen, the predictive capability of the hydrodynamic model is currently weakened due to the insulating surface layer of ice and snow.

It is postulated that a scene encompassing a partially frozen cooling lake will have various phenomena that will be observable through different imaging approaches. The first observable will be an ice-free zone present at and around the heat outflow location. The existence, size, and extent of this ice-free zone will depend on several factors including, but not limited to, lake bathymetry, weather conditions, exit mass flow rate, temperature of heat effluent, etc. It is desired that a correlation can be produced between the size of the ice-free zone and the exit mass flow rate of the given site, in the presence of accurate weather data. Infrared imagery as well as oblique wide-angle imagery is proposed as a solution for determining the aerial extent of the ice-free zone.

In addition to inspecting the ice-free zone itself, the remaining pond area covered by ice is the second observable of interest. The ice and snow present in these locations will significantly affect the ability of an

Further author information: E-mail: mva7609@cis.rit.edu, Telephone: 1 585 730 9682

imaging solution to determine any type of thermal information pertaining to the water surface directly below. It is suspected that ice and snow on the cooling lake will behave as insulators on top of the water surface. Two physical properties that are expected to be instrumental in the characterization of this interface as insulators are the thickness of the ice and the thickness and density of any present snow.

2. BACKGROUND AND THEORY

2.1 ALGE Model

ALGE is a 3-D hydrodynamic model developed by SRNL as part of the Multi-spectral Thermal Imager (MTI) project.[1] ALGE was originally developed, using thermal imagery as a model input, to simulate power plant cooling lakes and other methods used to eliminate waste heat such as cooling canals or direct discharge to rivers or the ocean. Situations in which ice formation occurred were not considered in the original version of the code. Thermal imagery provides a unique method for observing the thermal waste heat injected into a cooling pond by offering a complete spatial view of the thermal plume at a given instance in time. Additional required inputs into ALGE are the site specific weather and the cooling pond bathymetry.[2] In figure 1 are simulated surface temperature maps for a series of ALGE model runs for the same pond over varying weather conditions.

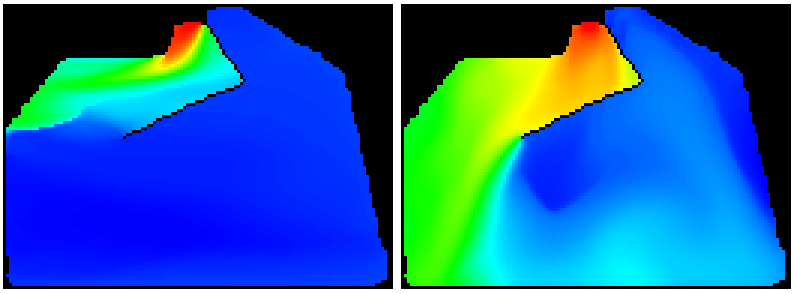

(a) (b)

Figure 1. ALGE surface temperature predictions for the Midland Cogeneration Venture cooling pond in Midland, MI using historical weather information.

The ALGE code optimizes the mass flow rate prediction for a given lake and weather conditions by incrementally changing the power generation facilities operating parameters. The rate at which the thermal waste is discharged into the pond can be used in subsequent engineering process models to predict operating power levels for the power generation site. A predicted thermal plume is output for each combination of parameters and is compared to the observed thermal plume image. The parameters used to produce the thermal plume prediction that is most similar to the observed thermal plume are designated as the hypothesized plant operational parameters.

3. EXPERIMENT

The data campaign for the winter of 2008-2009 was segmented into two major branches: the aerial data collection and the ground truth collection. While the aerial data collection has a single node of collection, the ground truth collection was a multi-faceted venture involving both manual and automatic measurements of water surface temperature, ice thickness, and weather conditions. Five buoys were deployed in the cooling lake of the Midland Cogeneration Venture (MCV) located in Midland, Michigan, while a weather station was constructed on the shore. The buoys as well as the weather station took automatic measurements of various parameters of interest and transmitted the data on daily intervals via cellular modems. In addition to the constant monitoring provided by the buoys, manual, high-density surface temperature measurements and ice thickness measurements were taken immediately following imagery collects. Flights were attempted on a weekly interval, as weather permitted.

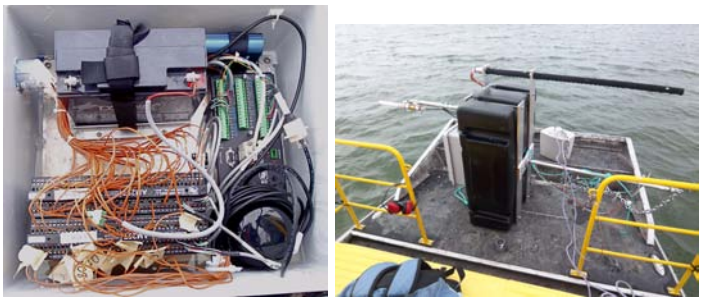

(a) Internal buoy components (b) Ice thickness probe

Figure 2. Inside of buoy containing datalogger, multiplexors, GPS units, battery, and cellular modem shown in 2(a). Ice thickness probe (long, black pole) mounted on side of buoy shown in 2(b)

3.1 Ground Truth Collection

Five identical buoys were deployed within the lake. Each buoy is equipped with a Campbell Scientific CR1000 datalogger to perform all data acquisition as well as control all telecommunications and GPS monitoring. The internal components of a constructed buoy is show below in figure 2(a).

The CR1000 monitored two different deployments of thermocouples used to measure the temperature profile of the water and ice thickness. The temperature profile thermocouples were attached to the mooring chain at one-foot increments and were queried by the datalogger at 30-second intervals. Every five minutes an average temperature value at each thermocouple was calculated and recorded. The second set of thermocouples was attached to a metal pole, at approximately 1-inch increments, beginning at the base of the buoy. These high-density thermocouples measured the temperature of either water or ice every 30 seconds with an average temperature recorded every five minutes. In addition to the main measurement systems on the buoys, twelve Tidbit dataloggers are attached to the chain of each buoy to serve as a backup temperature measurement system. Figure 3 shows the buoys deployed in both water and snow conditions.

(a) Buoy floating in open water (b) Buoy embedded in ice and snow

Figure 3. Buoys in both open water and iced conditions.

A single weather station was located near the hot outflow of the power plant. The weather station was constructed entirely from Campbell Scientific products. A Campbell Scientific CR3000 datalogger queries all individual weather modules at 30-second intervals and records averages and instantaneous values, depending on the module, at five-minute intervals. All recorded data is stored into data files that are transmitted twice daily (noon and midnight) via the same communication method as the buoys. Data recorded by the weather station includes air temperature, relative humidity, precipitation amount, wind speed, wind direction, shortwave irradiance, longwave irradiance, and barometric pressure. The constructed weather station is shown in figure 4(a).

(a) Weather station constructed on cooling pond shore

(b) Airboat used for data collections

Figure 4. Weather station and airboat used in Midland, MI in support of data collection campaign

Due to the strong dependence of ground truth collection on favorable weather conditions, a RIT ground team was stationed in Midland, MI at all times for the duration of the experiment period. Data collected by the ground truth team includes localized relative humidity, water surface temperature, ice thickness, snow thickness, and any presence of slush beneath the snow. All ground truth measurements were made from an airboat, shown in figure 4(b), in order to minimize the chance of any personnel injury on thin ice regions of the lake.

The airboat offers the unique ability to not only drive on water but also on ice. In lieu of making ice and snow measurements from the boat, transects of data were also collected by walking onto the ice from the shore of the lake. All water temperature data was recorded immediately following the collection of aerial imagery. It was impossible to collect surface temperatures concurrently with the flight time due to the thermal influence the airboat would have on the surface temperatures of the exposed water. It is assumed there was approximately a 1-2 hour window following the imagery collection where any collected surface temperature was valid. Ice and snow measurements are made either immediately before the flight or after the water temperature collection. It was assumed the collection of this data was not as temporally dependent as water surface temperature.

3.2 Imagery Collection

RIT's Wildfire Airborne Sensor Program (WASP) sensor, shown in figure 5, is a multi-spectral aerial mapping system with broad band coverage in the infrared and visible spectrum. Built by the RIT Laboratory for Imaging Algorithms and Systems (LIAS), WASP utilizes direct georeferencing hardware and processing techniques to create orthorectified imagery on-the-fly as the sensor is flown over the target scene. A recent upgrade to the system has enabled the generation of calibrated midwave and longwave infrared imagery.

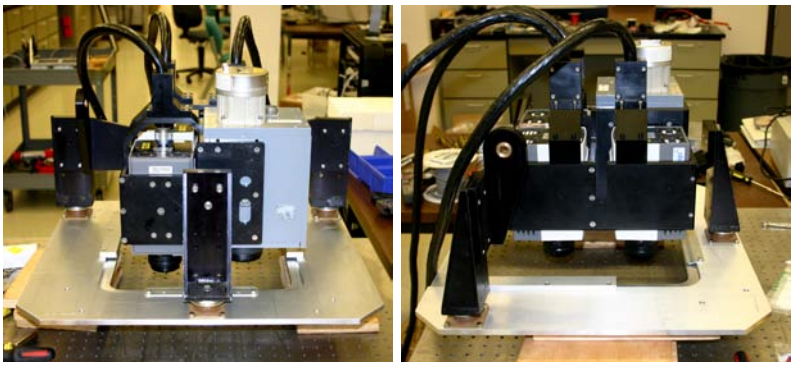

Figure 5. WASP sensor in laboratory

Originally designed as a fire detection and mapping system, WASP was built with three 640x512 pixel infrared cameras covering $0.9\mu m$ -$1.7\mu m$, $3\mu m$-$5\mu m$ and $8\mu m$-$9.2\mu m$; this spectral coverage allows the use a multi-spectral technique for positively detecting the presence of a wildfire in the imaged scene. Each infrared (IR) camera has a 25 micron pixel pitch and a lens with an approximate focal length of 25mm. The system also carries a 4096x4096 pixel RGB camera with a 9 micron pixel pitch and 50mm lens; this camera provides higher resolution visual coverage of the mission area. While not metric by design, each camera's optical system is stabilized for flight conditions and is geometrically modeled for lens distortion, principle point offsets, and focal length. To enable the creation of orthophotos by direct georeferencing, an Applanix POSAV-310 is utilized to record attitude information during the mission's flight. The POS's Litton LN-200 inertial measurement unit (IMU) is rigidly mounted to the camera frame assembly and boresight alignment angles for each camera are applied to generate exterior orientation parameters for each exposure station. Boresight angles for each camera are developed through a traditional bundle adjustment process utilizing imagery flown highly overlapped over a surveyed control point field.

All image and metadata from the mission flight are recorded by a rack-mounted computer system on solid state removable media, shown in figure 6(a), allowing for a service ceiling of at least 20,000 feet (tested) and high reliability without the use of specialized sealed hard drive enclosures. The WASP automated data processing computer (ADP) has the ability to orthorectify imagery on the fly as it's collected utilizing real-time exterior orientation solutions calculated by the POS and an archived digital elevation model of the area. Real-time generated orthos typically tie together acceptably for tactical applications and are absolutely accurate to about 4 meters rms; this data can be transmitted to ground observers via a high bandwidth RF data link. Once the plane lands, the raw recorded data can be further refined in a post-processing workflow yielding directly georeferenced ortho images absolutely accurate to better than 0.5 meters rms.

(a) WASP rack-mounted computer system

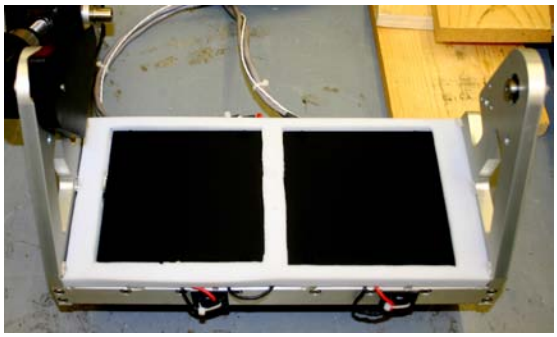

(b) Both blackbody sources

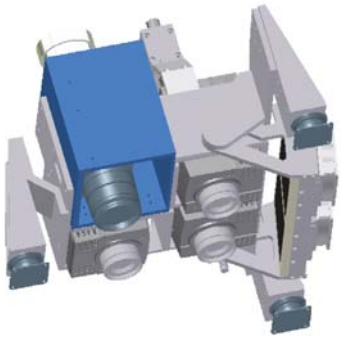

(c) AutoCAD image of WASP with blackbodies

Figure 6. WASP sensor with blackbody reference sources.

MWIR and LWIR array cameras are inherently susceptible to changes in environment that manifest as non-uniformities in the collected imagery. Most commercial IR camera systems provide mechanisms to perform uniformity corrections in a fixed environment; these procedures are not practical when applied to a constantly changing environment aboard and aircraft. In a recent upgrade to WASP, two thermoelectric plate blackbody reference sources were included in the design to address these issues. During a typical flight, the calibrators are moved to fill the field of view of the camera and imaged at two temperatures that bracket the scene to be mapped, typically at the beginning and end of a flight line. Imagery and temperatures gathered during the calibration process are used to post process imagery from the MWIR and LWIR cameras to perform a non-uniformity correction and calibrate the images to sensor reaching radiance. The blackbody sources and their configuration on WASP are shown in figure 6(b) and 6(c).

4. RESULTS

4.1 Ice thickness probe

Attached to each deployed buoy was an ice thickness probe consisting of 46 evenly-spaced thermocouples. Temperatures were recorded at each thermocouple and associated to their position relative to the top of the probe. Although designed so the first thermocouple would be approximately at water level, the actual location of this data point relative to the ice surface varied based on freezing conditions. The overall thickness of ice (if present) was determined by assuming any thermocouples registering temperatures of 0° or below were imbedded in ice. It was understood that this method of ice thickness determination would have larger errors during the freeze and melt periods. In figure 2(b), shown in section 3.1, the ice-thickness probe can be seen attached to the side of the buoy.

In order to determine the validity of this method ice holes were periodically drilled in close proximity to buoys that had been frozen in ice and the true thickness of the ice was measured. An ice thickness value is obtained from recorded buoy data through visual inspection of the thermocouple output. Below in figure 7 are four examples of plotted ice probe output. Figures 7(a) and 7(b) show the depth versus temperature recorded for the same buoy, Shiva, on two different days. Figures 7(c) and 7(d) shows the analogous information for a second buoy, Surya. It is important to note that on buoy Surya there was an inoperable thermocouple at the 17 inch mark.

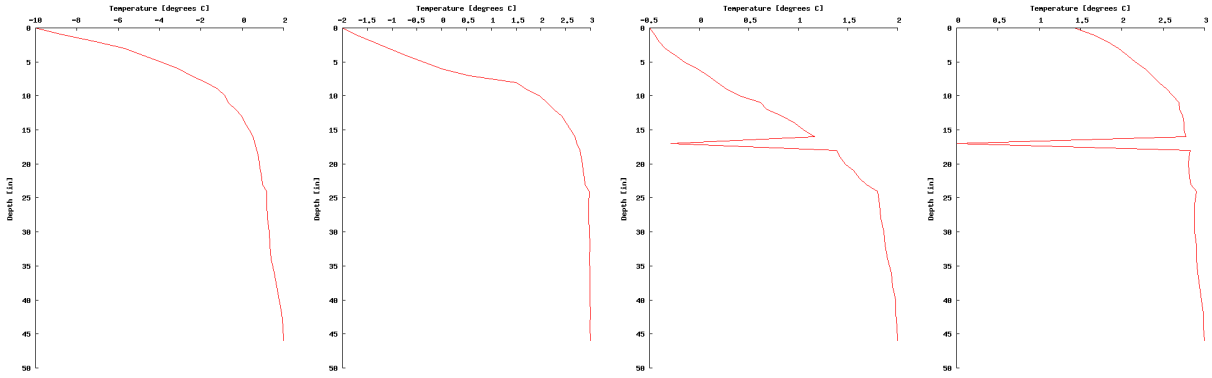

(a) Shiva buoy 1/14. (b) Shiva buoy 2/3 (c) Surya buoy 1/14 (d) Surya buoy 2/3

Figure 7. Plotted thermocouple output from ice thickness probe.

From visual inspection it is assumed that the first visible inflection point marks the first ice (or snow) interface with air. The second inflection point is designated the ice/water interface. The difference between these two points is calculated as the ice thickness. The images in figure 7 show the inflection points occuring at values higher than 0°. Due to manually observed and measured ice thickness values it is known that these plots do correspond to probes imbedded in ice. It is possible that the skew in temperature is a calibration issue with the thermocouples. In table 1 the comparison between manually and automatically measured ice thickness is shown.

Table 1. Measured ice thickness versus buoy-recorded ice thickness

Buoy	Measured by hand [in]	Recorded by buoy [in]	Snow depth [in]
Shiva 1/14	7.5	12	3
Shiva 2/3	11	16	0
Surya 1/14	9	9	4.5
Surya 2/3	13	8	2

There are several factors that could be responsible for the difference between manually measured and buoy observed ice thickness values. The buoy observed values are inferred from the thermocouple readouts at a specific time of the day. It has been observed that if the recorded thermocouple plots are viewed as a series of time-based frames in an animation the inflection points for the two surfaces are better defined and appear as

almost stationary points around which the bordering temperatures fluctuate. Performing a time series analysis to extract the interface points might lead to more accurate total thickness measurements. The presence of snow could also influence the thermocouple readings, particularly in windy conditions. Finally, it is not guaranteed that the buoys will freeze parallel to the water surface. As a result of this misaligned freezing the assumed depth resolution of the ice probe is no longer valid and the angle of the imbedded probe would have to be known to accurately extract the true depths of each thermocouple.

4.2 Ice cover estimation from oblique wide-angle and infrared imagery

The sigma fisheye lens was mounted onto a Nikon D50 digital SLR and used to capture a time series of the cooling pond from a high vantage point. This camera system is capable of producing a 180° FOV image of the cooling pond in a single exposure. The resulting images have geometrical distortions introduced by the lens. To acquire the necessary parameters to remove the geometric lens distortion, a calibration cage maintained by the LIAS research group at RIT was imaged. A block bundle adjustment can be performed to solve for focal length, symmetric radial distortion, and de-centering distortion. The results of this adjustment were applied to the roof-top images using a program written in IDL. Each pixel was transformed onto a new grid based on the distortion coefficients. The image was then interpolated back onto a regular grid using a radial basis function. An example of this process is shown in figure 8. The pixels in the distortion free image that contain ice or water were identified by hand using the ROI tool within ENVI as shown by figure 9.

(a) Original from roof-top. (b) After de-fish process

Figure 8. Original image captured from roof-top with processed version with geometrical distortions from fisheye lens removed. It should be noted that pixels near the edges of image begin to exhibit correction errors. This is due to low point density of calibration grid at the edge of the FOV.

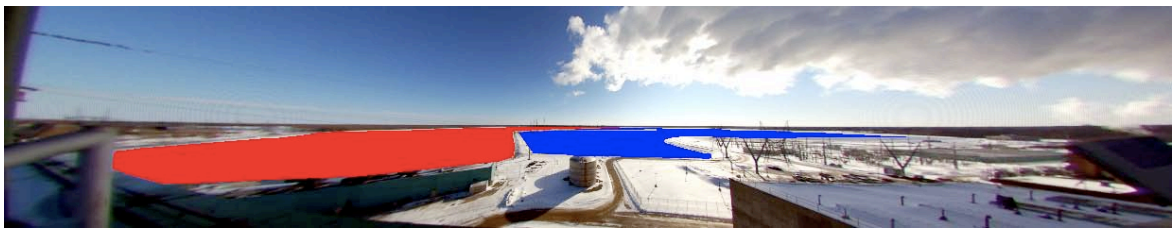

Figure 9. Ice and water pixels have been identified with two different ROI's. Water is tagged as blue, ice as red.

It should be noted that producing an automated algorithm to discriminate between water and ice pixels within oblique wide-angle imagery would be difficult. A large overlap in the pixel values exists between classes in all bands. Class confusion between the ice and water pixels could be the result of either shadowing from surrounding buildings driving the ice values closer to water or chromatic distortions resulting from interpolation errors. The interpolation errors are further exaggerated with oblique imagery because of the width of the resulting image grid. In addition, a major source of this issue is solar glint which drives many water pixel values close to ice values. Figure 10 shows the histogram for each band imaged for the ice and water classes. This issue could be resolved by using a multi-spectral instrument to improve the band separation.

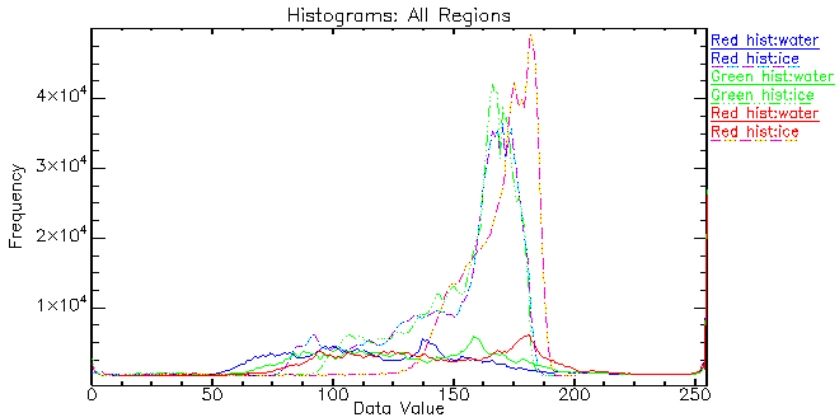

Figure 10. The water and ice classes overlap and are therefore very hard to discriminate into separate classes using conventional algorithms.

In order to determine the area of each pixel from the undistorted image, the location of the horizon needs to be found in each image. The distance from the center of the image to the horizon is found using edge detection. A region of interest is drawn which contains the horizon. Within this region a 'rake' of vertical lines are created. The points which contain the strongest falling edge (from bright sky to dark horizon) are found and then used to find the horizontal best fit line as well as the angle of the line relative to the x-axis. This process is implemented in the Labview environment which contains many useful tools for edge detection. The geometry of the image and its content is shown in figure 11(a).

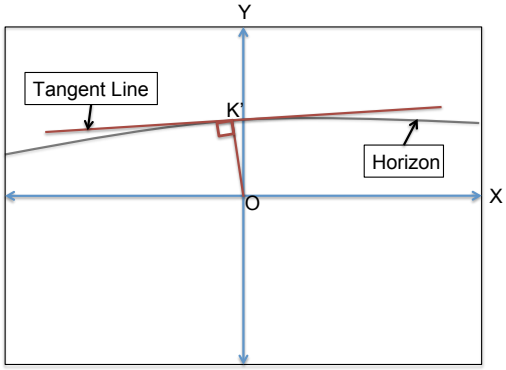

(a) Horizon geometry

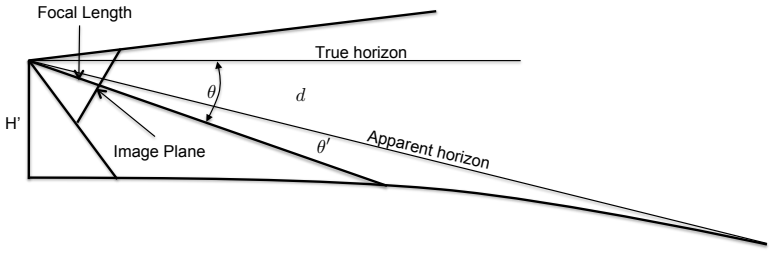

(b) Side-view geometry

Figure 11. Tangent line needed for calculations of scale shown in 11(a). Length OK' and the angle of the tangent line relative to the X-axis are needed. Side view of principle plane of the oblique photograph shown in 11(b).

To convert each pixel into a unit of area three things need to be known: the height of the camera relative to the pond surface (H'), the focal length of the lens (f), and the true depression angle (θ). The true depression

angle is measured from the camera optical axis to the true horizon line. The geometry is shown in figure 11(b).

H' is found by comparing the height of the building to the pond surface using hand-held gps units. The focal length is an output of the lens correction routine. The true depression angle, θ, is calculated using equations and a process described by Wolf.[3] Once H' and θ are found these parameters are used to rotate and translate the image so that the center origin of the image aligns with true horizon and is parallel to the x-axis. For each pixel the lengths along the vertical (Δy) and horizontal (Δx) sides are calculated in pixel units from two of the pixel's corners. Both lengths (Δx, Δy) are projected into the world plane and translated into arbitrary world coordinates (see equations 1 and 2). It should be noted that the pixel shape will be distorted from a square into a polygon. However since the camera height is small relative to most airborne scenarios, the error introduced into the area calculation is assumed to be small. The area is now found by: $A = \Delta X \cdot \Delta Y$.

$$\Delta X = \Delta x \left(\frac{H'}{|y_h| cos\theta} \right) \tag{1}$$

$$\Delta Y = \left(\frac{1}{y_l} - \frac{1}{y_h} \right) \left(\frac{f H'}{cos^2\theta} \right) \tag{2}$$

The results for the images collected in which there was ice present are described below in table 2.

Table 2. Calculated Ice and Pond Area (acres) from Oblique

Date	Total Area	Water Area	Ice Area
2/02/09	847.466	403.199	444.266
2/03/09	851.744	268.278	583.465
2/04/09	854.782	350.716	504.066
2/05/09	846.614	213.975	632.638
2/09/09	853.257	475.844	377.414
2/10/09	852.581	480.129	372.452
2/24/09	853.570	65.1202	788.450
2/25/09	855.080	245.198	609.882
3/04/09	853.722	444.044	409.678

A relevant error metric is to compare the area values obtained from the oblique images to those obtained from the LWIR imagery acquired with the WASP system. This comparison was possible for two sets of data, seen in table 3. These two data sets are successful because of the extreme difference between the ice conditions on both days. Images collected on 24 February 2009 show most of the pond uniformly covered in ice and therefore allows the user to create accurate ROIs in both the nadir and oblique images. Imagery collected on 4 March 2009 illustrate a variable ice distribution on the lake surface which is difficult to distinguish in the oblique imagery. Figure 12 shows each day used in the comparison as both an oblique image, a nadir LWIR image, and a nadir LWIR image with the open water ROI selected.

Table 3. Pond Area Comparison (oblique vs. nadir)

Image Type	Date	Total Area	Water Area	Ice Area
Oblique	2/24/09	853.570	65.1202	788.450
Nadir	2/24/09	853.810	79.270	774.540
Difference	2/24/09	0.24	14.150	13.910
Oblique	3/04/09	853.722	444.044	409.678
Nadir	3/04/09	854.182	373.389	480.793
Difference	3/04/09	0.46	70.655	71.115

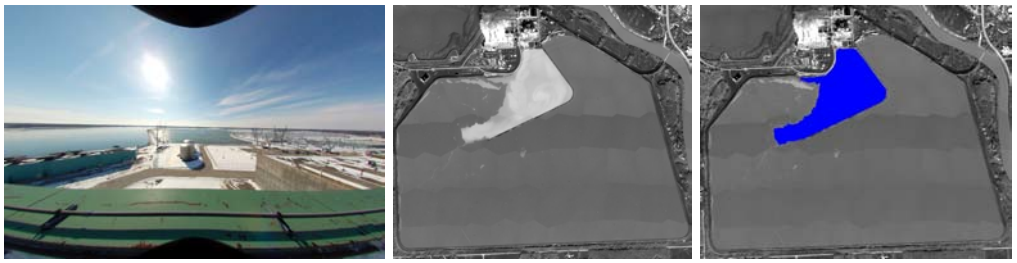

(a) 2/24/09 - Oblique (b) 2/24/09 - Nadir LWIR (c) 2/24/09 - Nadir LWIR with open water ROI

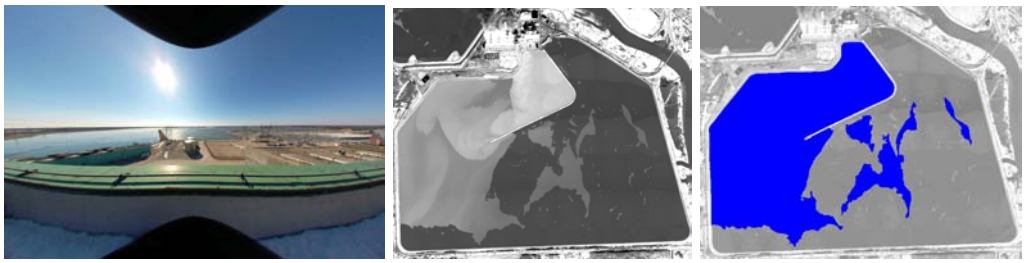

(d) 3/04/09 - Oblique (e) 3/04/09 - Nadir LWIR (f) 3/04/09 - Nadir LWIR with open water ROI

Figure 12. Images used in comparison and error metric calculations. Left-most image shows de-fished fisheye images. Middle images show nadir captured LWIR images used to select the open water ROIs for error comparison.

4.3 ALGE model results

The 3-D hydrodynamic model has been extended to include a 1-D ice formation model. Ice thickness and thickness distribution on the cooling pond is not only affected by local weather and the pond bathymetry but also the forced water circulation beneath the surface, presence of snow on the ice surface, and the solar radiation transmitted through the ice. ALGE is currently calculating the presence of ice and its associated thickness by assuming any node within the modeled pond having a temperature of 0° and below are ice and designating them as such. Figure 13 show six simulated surface temperature maps, using historical data, for the MCV cooling pond. The uniform areas of blue in the simulations represent predicted ice locations. The images are presented in clockwise chronological order and illustrate the predicted ice build-up on the pond.

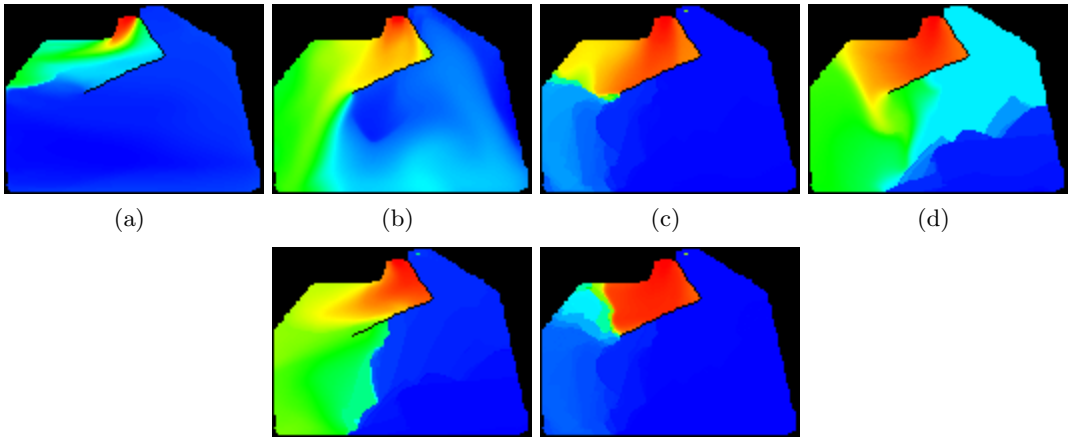

(a) (b) (c) (d)

(e) (f)

Figure 13. ALGE surface temperature predictions for the Midland Cogeneration Venture cooling pond in Midland, MI using historical weather information. The uniform areas of blue indicate the presence of ice at those locations.

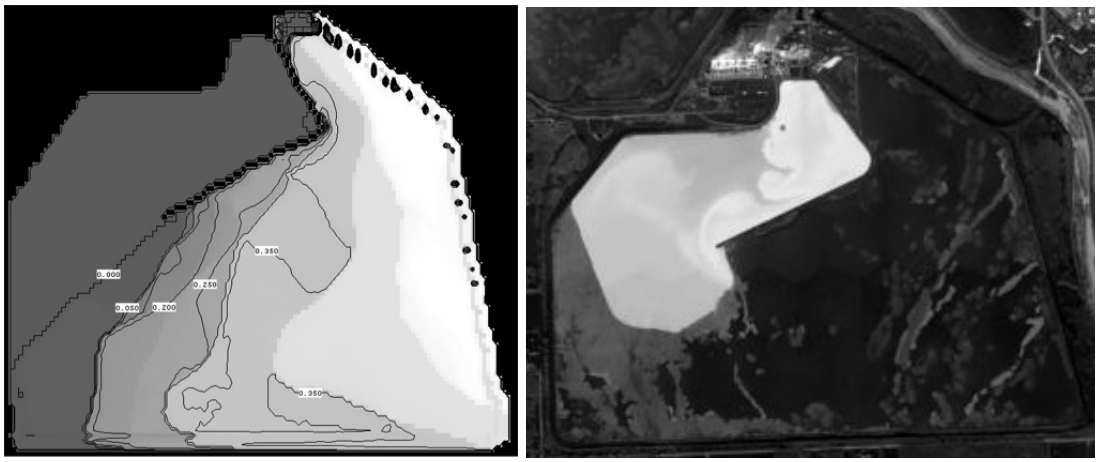

(a) ALGE simulated ice thickness for 1/22/09 (b) LWIR WASP imagery from 1/24/09

Figure 14. Comparison of ALGE predicted ice thickness and observed pond surface conditions using WASP

In figure 14 an ALGE produced thickness map is compared to collected LWIR imagery. It is important to note that the simulation is for 22 January 2009 and does not include snow while the image was captured 24 January 2009 and snow was present.

Visual comparison of the two images indicate an error between the simulated ice cover fraction and the actual amount of ice cover present on the pond. However this discrepancy between the model and observed can most likely be attributed to the lack of consideration given to snow cover in the simulation and the difference in date.

Snow presence on an ice surface will produce a high degree of uncertainty in the heat transfer from the ice surface to the atmosphere due to snow's highly variable thermodynamic and radiative properties. In figure 15 the blue curve shows ALGE's predicted ice thickness while the red curve shows the predicted ice thickness when covered with snow. Furthermore, figure 16 demonstrates the effect the presence of snow has on the overall fraction of the pond covered with ice, as simulated with ALGE. Clearly the presence of snow dramatically affects the ice formation and requires further investigation.

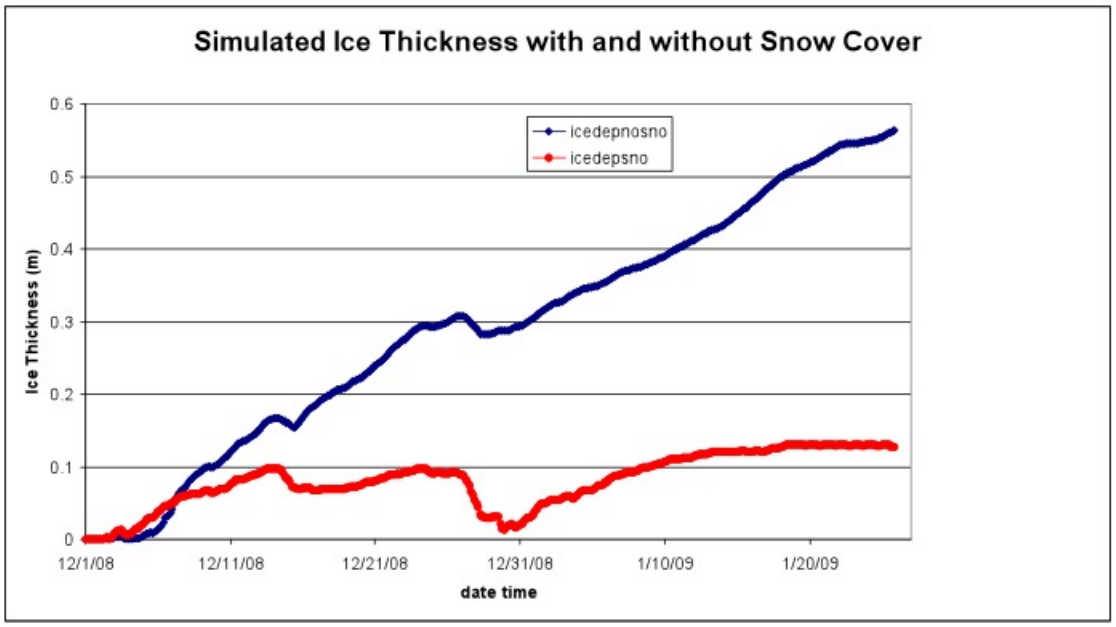

Figure 15. ALGE's predicted ice thickness with the presence of snow (red curve) and without snow (blue curve).

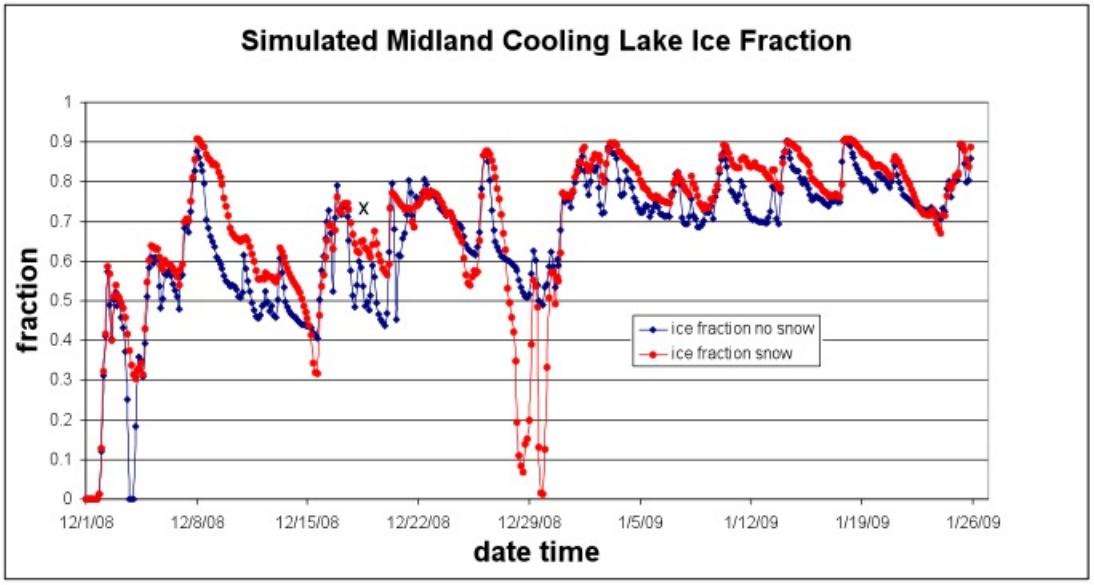

Figure 16. ALGE's predicted ice fraction for entire pond with (red curve) and without (blue curve) snow.

5. CONCLUSIONS

It can be concluded that aerial thermal imagery is key to improving the validity the 3D hydrodynamic code, ALGE, when extending the model to include ice formation. In particular knowledge gained pertaining to the location any ice/water boundaries is a crucial test to the accuracy of the model. It has been shown that ice thickness is variable and significantly impacted by not only weather and lake bathymetry, but also the presence and depth of any snow. Further improvement to the overall design of the buoys for the given environmental conditions will be performed with an aim to improve the accuracy of ice thickness observations. Due to the significance ice and snow pose to the thermodynamic balance of the cooling pond future work will investigate methods for remotely determining snow depth and ice thickness.

REFERENCES

1. A. J. Garrett, "Analyses of MTI imagery of power plant thermal discharge," *Imaging Spectrometry VII* **4480**, pp. 264–273, SPIE, Jan 2002.
2. A. Garrett and D. Hayes, "Cooling lake simulations compared to thermal imagery and dye tracers," *Journal of Hydraulic Engineering* **123**, p. 885, 1997.
3. B. A. D. Paul R. Wolf, *Elements of Photogrammetry (with Applications in GIS)*, McGraw-Hill Science Engineering, 2000.